

NATIONAL RADIO ASTRONOMY OBSERVATORY

12 M TELESCOPE

RECEIVER AND CALIBRATION STATUS

MAY 1988

I. Introduction

This report summarizes the current status of equipment and system calibration at the NRAO 12 m telescope. The following two sections give some general comments about equipment and calibration; the figure captions give detailed information about each of the graphs displayed. This report will be updated on a regular basis as the equipment and system calibration status changes. Before using the information contained in this report, check with the NRAO Tucson staff to see that you have the most recent version.

II. Receiver Status

The receivers available for general use at the 12 m are listed in Table 1, The NRAO 12 m Front-End Box Status Sheet. For each receiver, the table lists the frequency coverage, the amplifier type, a typical receiver noise temperature, the continuum sensitivity for each polarization channel, the bandwidth, the feed type, polarization of the feed(s), the calibration system, any remarks, and the engineer in charge of maintaining the receiver.

Graphs of the receiver noise temperatures as a function of frequency are presented in Figures 1 - 4 for four Schottky receivers. Because the majority of observations done on the 12 m are of spectral lines, the noise temperatures are referred to the single sideband (SSB) scale. The Schottky receivers are, in fact, all double sideband (DSB) systems with no inherent sideband rejection. The noise temperatures are measured on the DSB scale. We assume, with some confidence, that the gains of the image and signal sidebands are equal and thus derive the SSB temperatures by doubling the DSB temperatures. Continuum observations are usually performed as DSB observations. Continuum sensitivity is often determined by low frequency excess noise rather than the noise temperature, however. Continuum sensitivities are listed in Table 1.

Some of the noise temperatures were measured in the laboratory and some were measured on the telescope. The laboratory measurements were made through most or all of the receiver optics (in particular, the lens-corrected feed system and L.O. diplexer), and are representative of the values an observer will obtain with a hot/cold load measurement on the telescope. Measurements made on the telescope are made by holding hot and cold loads above the window to the receiver box.

The noise temperatures of two receivers are not plotted as a function of frequency. We have not had an opportunity to measure systematically the noise temperatures of the 90-115 GHz SIS receiver since the current mixer junctions have been installed. Spot checks indicate that the noise temperatures in each receiver

channel vary between 80 and 150 K across the band. No evidence of any "holes" in receiver performance has been found. The SIS receiver can be tuned as a single sideband or double sideband system. For spectral line work, the receiver is almost always tuned for single sideband operation.

The other receiver for which we do not have detailed measurements is the 330 - 360 GHz receiver. The receiver has been tuned across the band, however, and appears to have noise temperatures ranging between 1800 and 2200 K (SSB). The best performance is at the middle of the band, 345 GHz, with some rise in noise toward the edges of the tuning range.

Note that the numbers plotted are receiver temperatures, not system temperatures. The effective system temperature is defined as

$$T_{\text{sys}}^* = \frac{T_{\text{Rx}}[\text{SSB}] + (1 + G_i/G_s)T_A[\text{sky}]}{\eta_t \eta_{\text{fss}} \exp(-\tau)},$$

where G_i and G_s are the image and signal sideband gains, respectively, T_{Rx} is the measured receiver temperature using broadband hot and cold loads, η_t and η_{fss} are the rear and forward spillover efficiencies (see Section III), and τ is the atmospheric optical depth at the position of the observation. $T_A[\text{sky}]$ is the antenna temperature of the sky, defined as

$$T_A[\text{sky}] = \eta_t T_M [1 - \exp(-\tau)] + (1 - \eta_t) T_{\text{spill}} + \eta_t T_{\text{bg}} \exp(-\tau).$$

In the equation above, $G_i/G_s = 1$ for a double sideband tuning and $= 0$ for a single sideband tuning, T_M is the mean atmospheric temperature, T_{spill} is the spillover temperature, and T_{bg} is the cosmic background temperature. Additional information about the receivers is given in the Figure Captions.

All 12 m coherent receivers use Gunn oscillators as local oscillator (L.O.) sources. Although most of the Gunns have broad tuning ranges, observing programs utilizing a wide range of frequencies may require more than one Gunn oscillator. We have included the coverage of the L.O. sources for the 3 mm, 1.2 mm, and 870 μm bands. Note that the 1.2 mm receivers (200 - 310 GHz) use a tripler and the 330 - 360 GHz receiver uses a quadrupler.

A calibration curve for the throw of the nutating subreflector is also included. This curve will change if the control electronics are adjusted. The nutating subreflector is used for beam switched observations in both spectral line and continuum modes. This curve will be of use in varying the throw of the subreflector. The range of the throw is 0 - 6 arc minutes and is always switched in azimuth.

III. Calibration Status

This section gives efficiency and calibration parameters for the 12 m telescope as they are presently understood. The aperture efficiencies and the corrected beam efficiencies have been measured at several standard frequencies. From these measurements, we have parameterized the telescope in terms of Ruze theory. All efficiency measurements were made at the Cassegrain focus and include the losses of the feed and all optics. The Ruze parameters thus include the net effect of the entire telescope and receiving system, not just the primary reflector. Several of the graphs are not based on direct measurement but are inferred from Ruze theory. These curves are identified in the figure captions.

These calibration factors are intended for "first order" calibration of 12 m data and as an indication of system sensitivity in assessing the feasibility of observing programs. Observers requiring precise calibration should make calibration measurements at their specific observing frequencies. The NRAO staff will be glad to assist in these measurements. The calibration parameters of the telescope are listed in the following table.

12 m Telescope Parameters

Dish diameter	D	12.0 m
RMS surface accuracy	σ	77-85 μm
(see note below)		
Infinite wavelength aperture efficiency .	η_{AO}	0.52
Surface deviation correlation size	c_{σ}	28 cm
Feed taper function	κ	1.22
Forward Spillover Efficiency	η_{fss}	0.75
Rear spillover efficiency	η_l	
(70 - 310 GHz receivers)		0.85
(330 - 360 GHz receiver)		0.78

Note: A range of values are given for the RMS surface accuracy. The aperture efficiency is fit best by the larger RMS values while the beam efficiencies are fit best by the smaller RMS values. This is probably the result of the astigmatism associated with the primary reflector. The astigmatism tends to broaden the beam which will degrade the response to a point source more than for an extended source.

The numbers given above are appropriate for the conventional hyperbolic subreflector in use at the 12 m for the past several years. We are experimenting with a shaped subreflector that corrects for the dish astigmatism and other surface errors. In an initial trial, the subreflector produced a dramatic (60%) improvement in point source signal strength at 345 GHz. At this writing, the shaped subreflector has been removed for evaluation of its surface. We expect it, or an improved version, to be

reinstalled during the 1988 - 1989 observing season. This document will be revised at that time to reflect the improved performance of the dish.

A final figure included in this report shows how the 230 GHz gain of the telescope to a point source varies with elevation angle. For extended sources, the fall-off in gain may not be as sharp as for a point source. The measurements and the estimated best fit curve are plotted.

Figure Captions

- Figure 1** The single sideband receiver noise temperatures for the 3 mm Schottky mixer receiver in the 70 - 90 GHz band. This receiver has two separate mixer pairs, covering roughly 70 - 90 GHz and 90 - 115 GHz, respectively. The 90 - 115 GHz pair is still available, but has been superseded for almost all projects by the 3 mm SIS receiver.
- Figure 2** The SSB receiver noise temperatures for the 200 - 240 GHz mixers in the 1 mm receiver package. The 1 mm receiver box contains 4 dual polarization mixer sets (8 mixers in all) covering the range 200 - 360 GHz.
- Figure 3** The SSB receiver noise temperatures for the 240 - 270 GHz Schottky mixer pair of the 1 mm receiver package.
- Figure 4** The SSB receiver noise temperature for the 270 - 310 GHz Schottky mixer pair of the 1 mm receiver package.
- Figure 5** The L.O. frequency range of the Gunn oscillators available for use with the 3 mm receivers (SIS and Schottky). The I.F. of 1.5 GHz allows signal sideband observations to extend another 1.5 GHz on either end of the plotted bars.
- Figure 6** The L.O. frequency range of the Gunn oscillators (and tripler) available for use with the 1.2 mm receivers (200 - 270 GHz).
- Figure 7** The L.O. frequency range of the Gunn oscillators (and quadrupler) available for use with the 270 - 310 GHz and the 330 - 360 GHz receivers.
- Figure 8** The calibration curve for the subreflector control dial as a function of measured beam throw on the sky. This curve is subject to change if the electronics are adjusted.
- Figure 9** The conventional aperture efficiency, defined by the relation

$$\eta_A = \eta_{A0} \exp(-\delta^2),$$

where
$$\delta = \frac{4\pi\sigma}{\lambda}.$$

Representative measurements of this quantity at several frequencies are plotted.

Figure 10 The conventional main beam efficiency, defined by the relation

$$\eta_M = \eta_A \frac{A_p \Omega_M}{\lambda^2},$$

where
$$\Omega_M = 1.13\theta_M^2,$$

and A_p is the physical aperture (113 m²).

This quantity was derived from the aperture efficiency and the theoretical FWHP beamwidth.

Figure 11 The main diffraction beamwidth (FWHM). This curve is plotted from the standard relation,

$$\theta_M = \kappa \frac{\lambda}{D},$$

where κ is the feed taper factor.

At high frequencies, the azimuth beamwidth is broadened beyond its theoretical width by the astigmatism of the primary reflector.

Figure 12 Janskys per Kelvin of T_A . This conversion factor is appropriate for converting point source antenna temperatures (standard calibration) to flux densities. If the source is extended relative to the beam, a beam resolution factor must be applied. Do not use this conversion for spectral line data calibrated by chopper wheel or vane. This curve is plotted from the relation

$$S_\nu/T_A = \frac{1}{\eta_A} \frac{2k}{A_p}.$$

where S_ν is the flux density.

Figure 13 Janskys per Kelvin of T_R^* . This quantity can be used to convert point source antenna temperatures measured on the vane or chopper wheel calibration scale, T_R^* , to flux densities. Measurements of this quantity at three different frequencies are plotted on the graph. This factor is given by the relation

$$S_{\nu}/T_R^* = \frac{\eta_t \eta_{rss}}{\eta_A} \frac{2k}{A_p} .$$

Figure 14 The corrected beam efficiency. This quantity can be used to convert a T_R^* temperature to a main beam brightness temperature, provided that the source is not extended beyond the main beam. The corrected beam efficiency is the fraction of forward power in the main diffraction beam relative to the total forward power in the main beam plus error beam. The quantity is given by the relation

$$\eta_M^* = \frac{1}{1 + \frac{A_E \theta_E^2}{A_M \theta_M^2}} ,$$

where A_E and A_M are the amplitudes of the error and main beams, respectively, and θ_E and θ_M are the FWHM of the error and main beams, respectively.

Figure 15 The FWHM of the error beam. This quantity has been measured at only one frequency; the plotted curve should be used only as a rough indicator of the extent of the error beam. The theoretical relation on which the curve was generated is given by

$$\theta_E = 2(\ln 2)^{1/2} \frac{\lambda}{\pi c_{\sigma}} ,$$

where c_{σ} is the correlation scale size of surface deviations.

Figure 16 The amplitude of the error beam relative to the amplitude of the main beam. As with the width of the error beam, this quantity is based on a theoretical estimate rather than hard measurement; use the curve only as a rough indicator of the relative amplitudes of the main and error beams. The theoretical relation on which the curve was generated is given by

$$\frac{A_E}{A_M} = \frac{1}{\eta_{A0}} \left(\frac{2c_{\sigma}}{D} \right)^2 (\exp(\delta^2) - 1) ,$$

where all the parameters have been defined above.

Figure 17 The variation of antenna gain with elevation angle at a wavelength of 1.3 mm. The data points and a fitted curve are plotted. This curve is valid only for point sources.

P. R. Jewell
20 May 1988

TABLE 1

NRAO 12 M TELESCOPE FRONT-END BOX STATUS
1988 MAY

APPLICABLE TELESCOPE	FREQUENCY (GHz)	AMPLIFIER TYPE	RECEIVER TEMPERATURE (KELVIN)	CONTINUUM SENSITIVITY (JANSKY /SEC)	3 dB BANDWIDTH (MHz)	FEED TYPE	POLARIZATION	CALIBRATION VALUE	SWITCHING SYSTEM	REMARKS	PERSON(S) IN CHARGE
12 M	70-115	COOLED SCHOTTKY	300-500 SSB	1.5	600	HORN-LENS	DUAL LINEAR	6 K	NUTATING SUBREFLECTOR		PAYNE
12 M	90-115	SIS	80-150 SSB	1.0	600	HORN-LENS	DUAL LINEAR	6 K	NUTATING SUBREFLECTOR		LAMB
12 M	200-240	COOLED SCHOTTKY	500-700 SSB	7.0	600	HORN-LENS	DUAL LINEAR	N/A	NUTATING SUBREFLECTOR	200-360 GHz receivers are contained in a single receiver box.	PAYNE
12 M	240-270	COOLED SCHOTTKY	900-1200 SSB	NOT MEASURED	600	HORN-LENS	DUAL LINEAR	N/A	NUTATING SUBREFLECTOR		PAYNE
12 M	270-310	COOLED SCHOTTKY	1100-1600 SSB	NOT MEASURED	600	HORN-LENS	DUAL LINEAR	N/A	NUTATING SUBREFLECTOR		PAYNE
12 M	330-360	COOLED SCHOTTKY	1800-2200 SSB	NOT MEASURED	600	HORN-LENS	DUAL LINEAR	N/A	NUTATING SUBREFLECTOR		PAYNE
12 M	220-240	COOLED SCHOTTKY	500-700 SSB	NOT MEASURED	600	8-BEAM HORN-LENS	LINEAR	N/A	NUTATING SUBREFLECTOR	8-Beam Receiver Under Development	PAYNE
12 M	5	ROOM TEMP. HEMT	100	N/A	100	HELIX	CIRCULAR	N/A	NONE	For VLBI use	PERFETTO

70 – 90 GHz Schottky Receiver Noise Temperatures

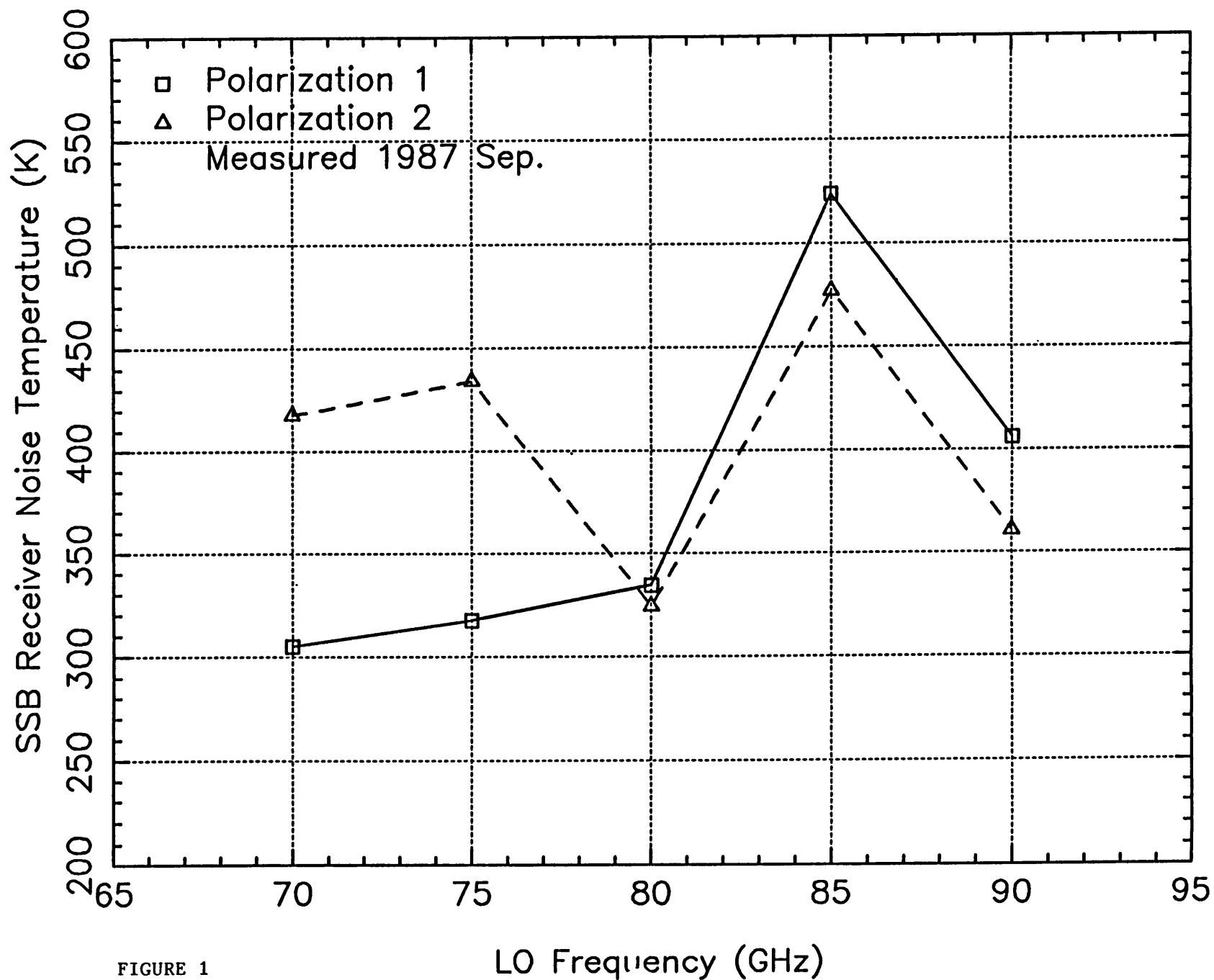


FIGURE 1

200 - 240 GHz Schottky Receiver Noise Temperatures

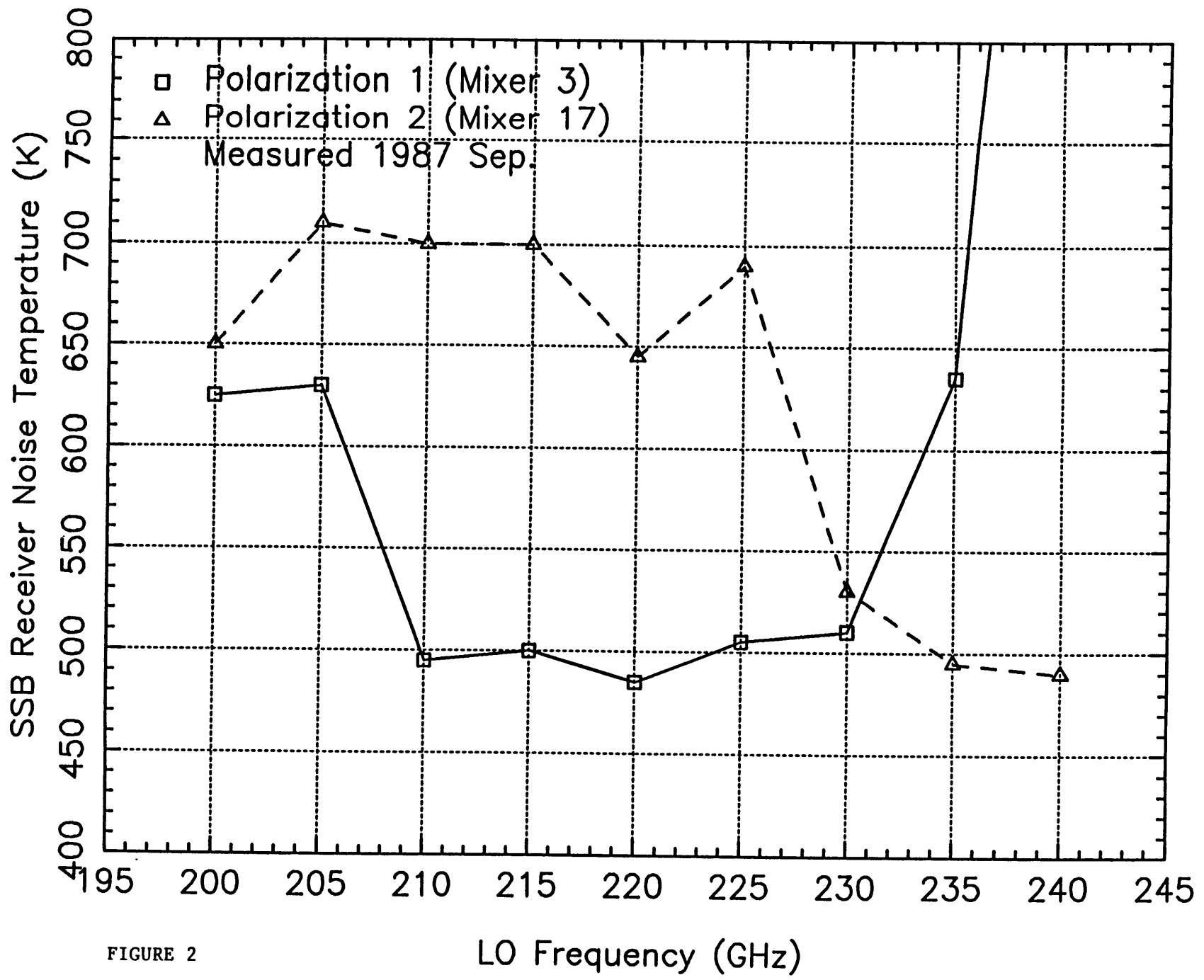


FIGURE 2

240 – 270 GHz Schottky Receiver Noise Temperatures

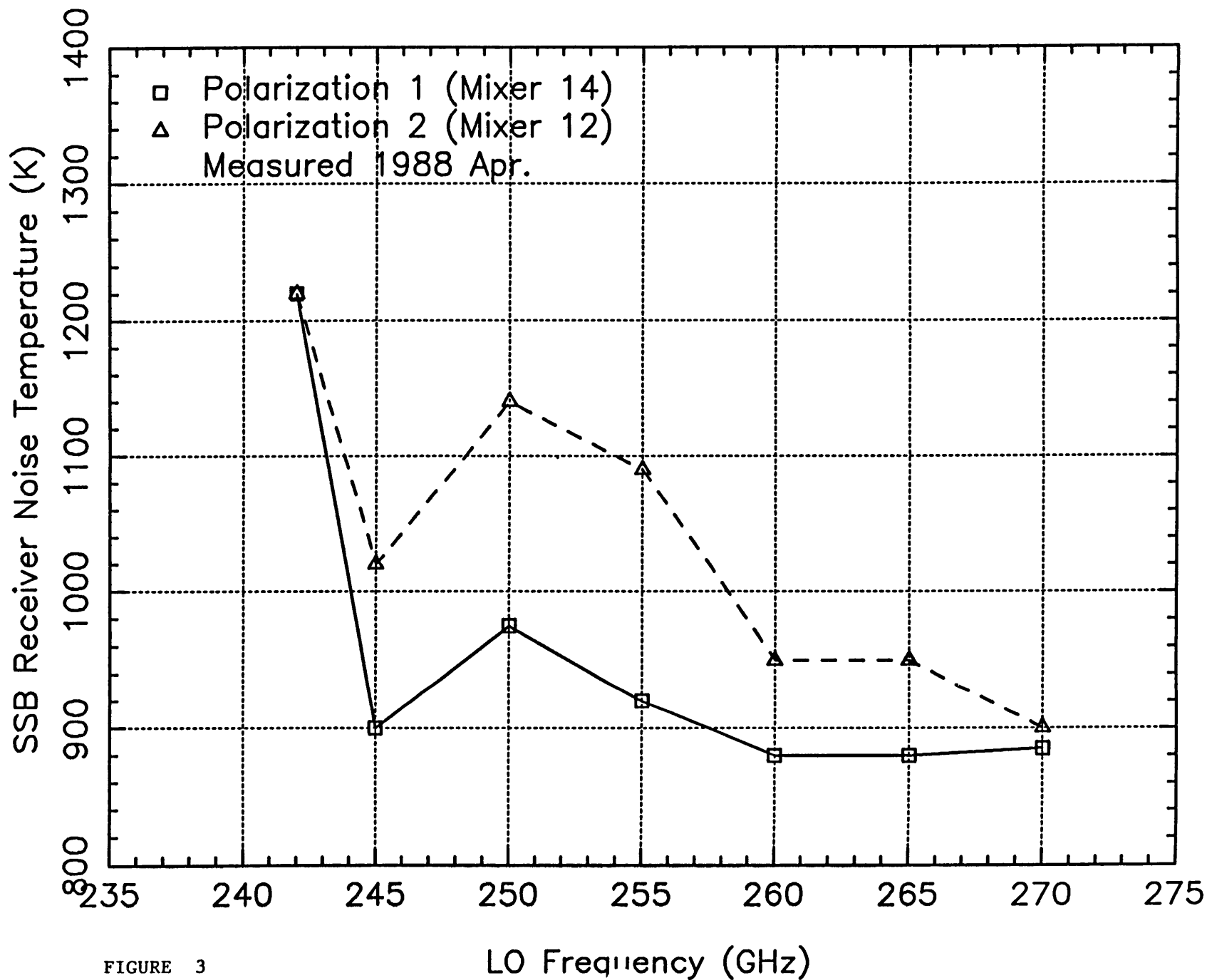


FIGURE 3

270 - 310 GHz Schottky Receiver Noise Temperatures

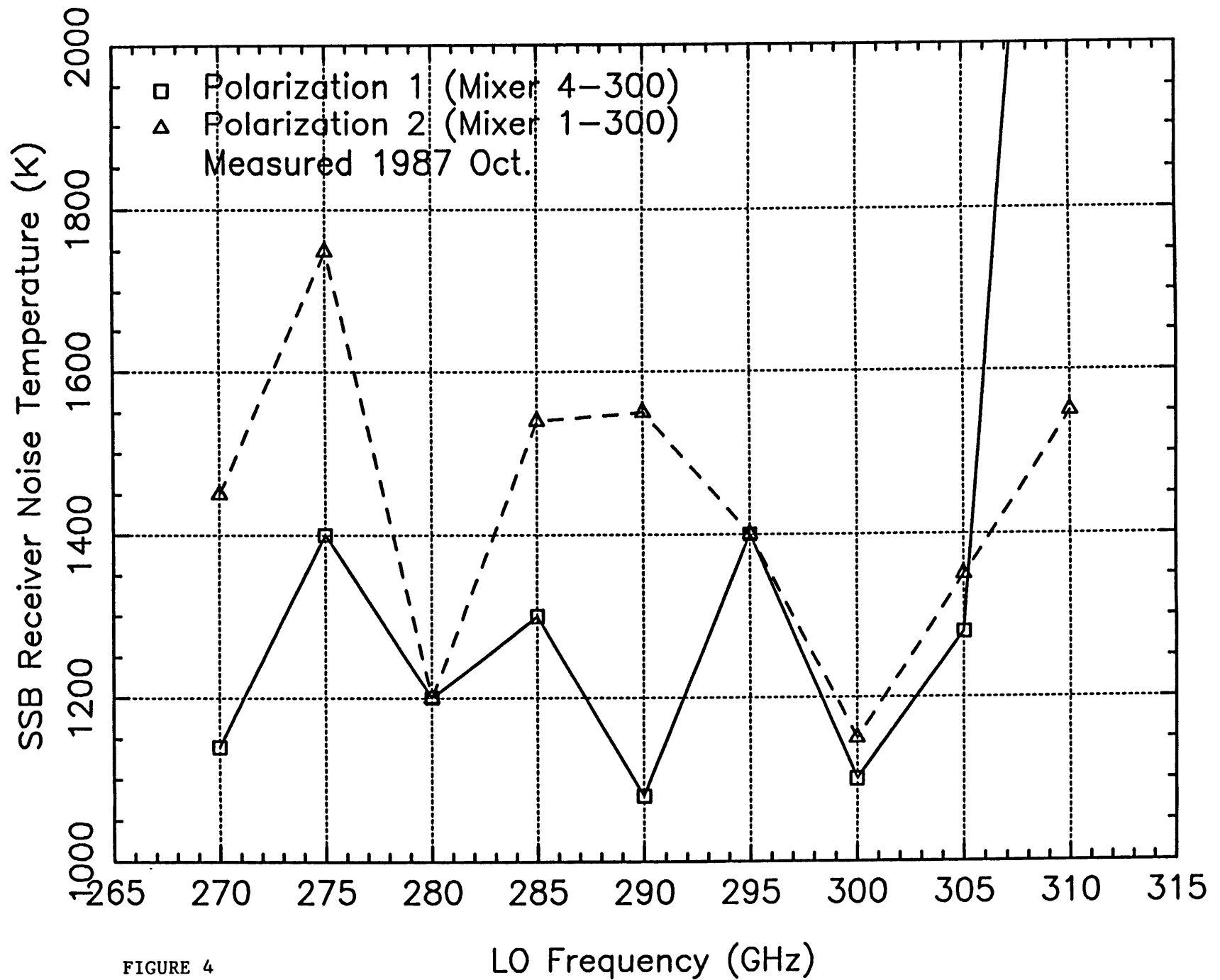


FIGURE 4

LO Frequency (GHz)

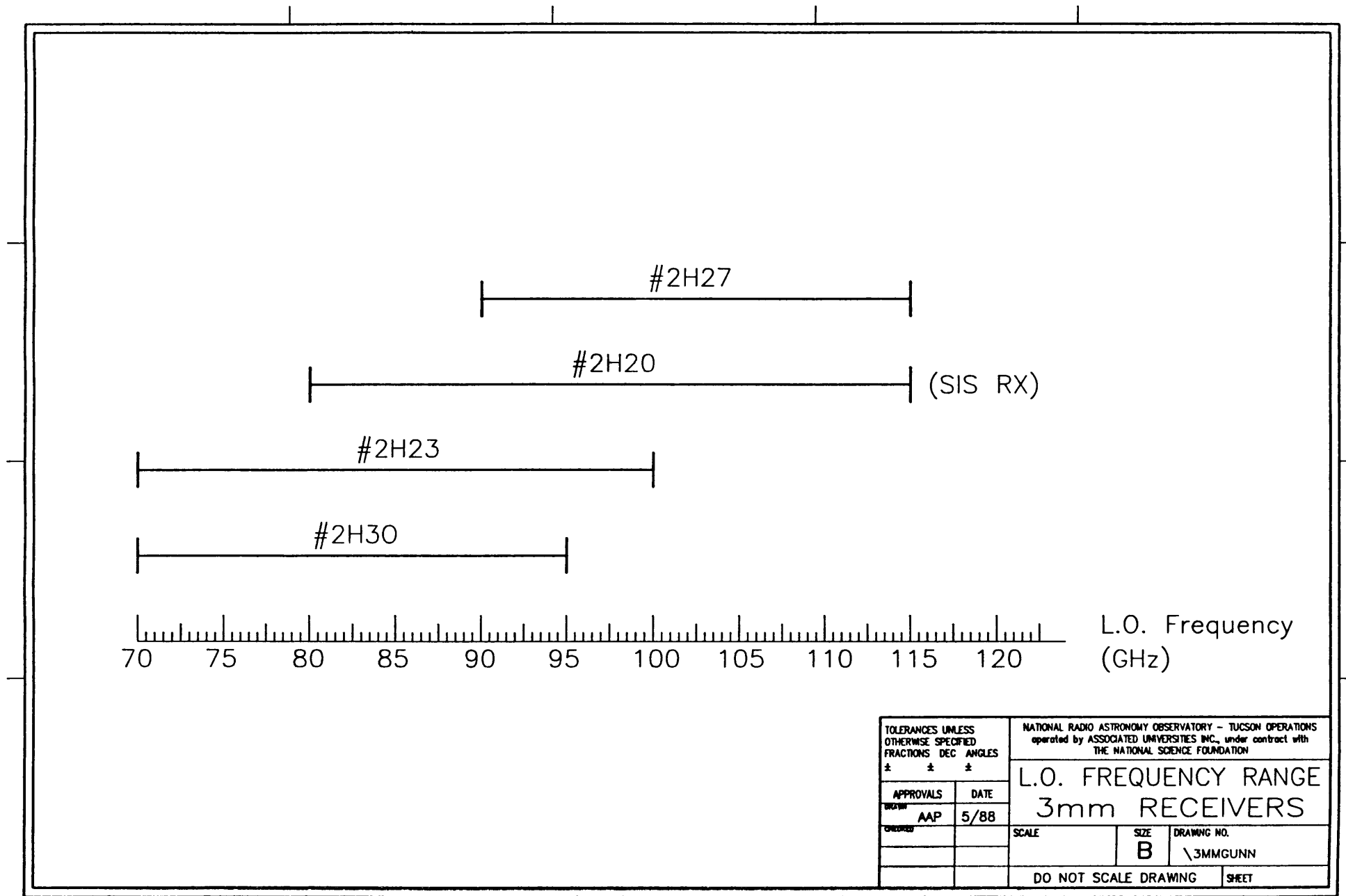


FIGURE 5

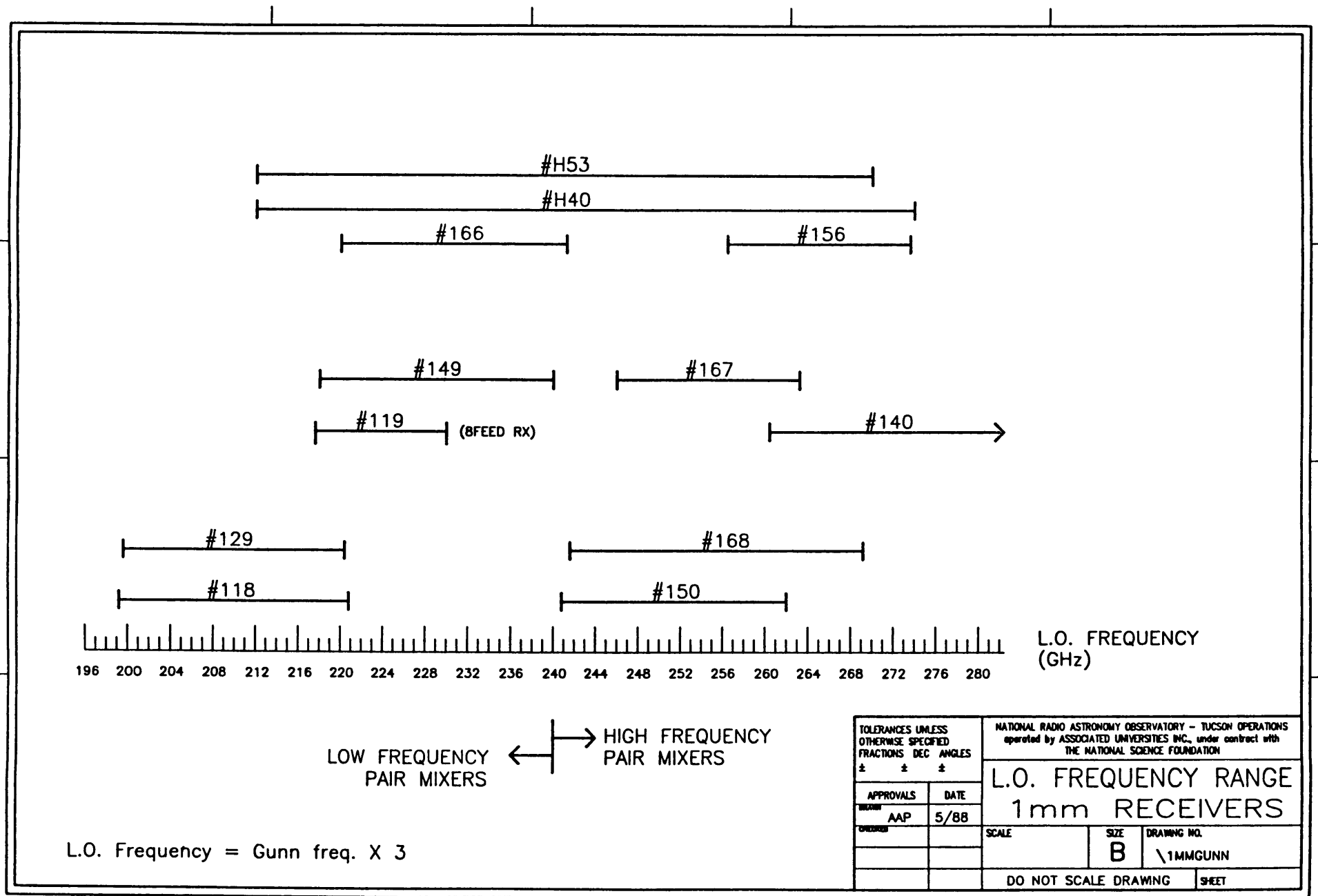
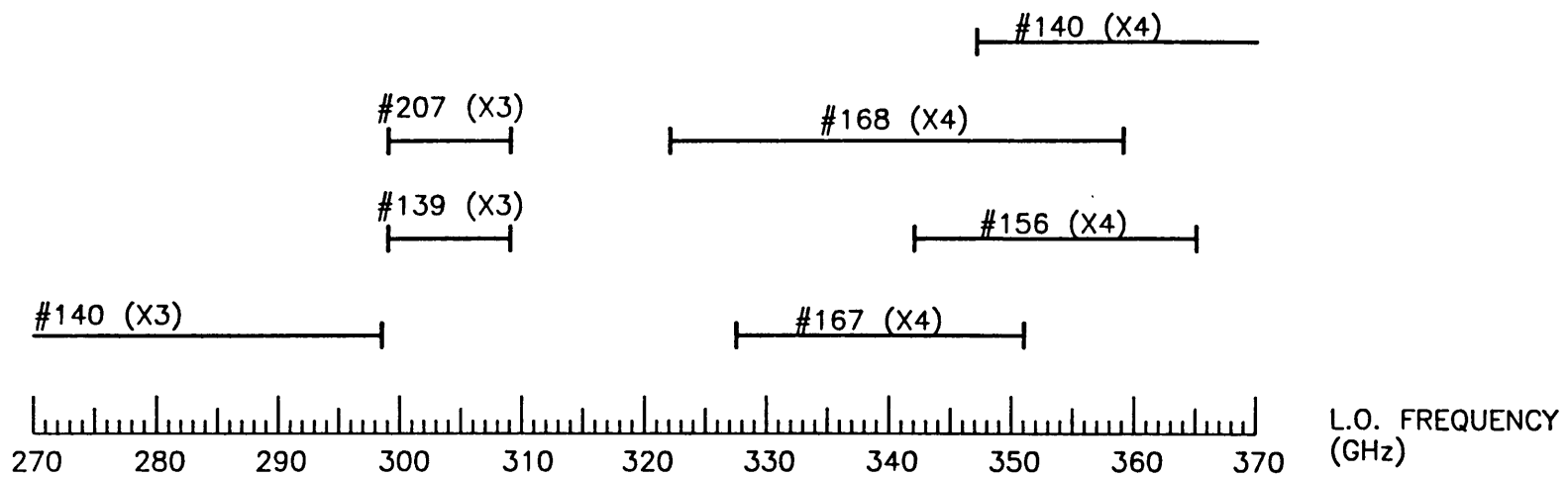


FIGURE 6



TOLERANCES UNLESS OTHERWISE SPECIFIED		NATIONAL RADIO ASTRONOMY OBSERVATORY - TUCSON OPERATIONS	
FRACTIONS DEC ANGLES		operated by ASSOCIATED UNIVERSITIES INC., under contract with THE NATIONAL SCIENCE FOUNDATION	
± ± ±		L.O. FREQUENCY RANGE	
APPROVALS	DATE	300/345 GHz RECEIVERS	
DRAWN AAP	8/88	SCALE	SIZE B
CHECKED		DRAWING NO.	\SUBMGUNN
DO NOT SCALE DRAWING		SHEET	

FIGURE 7

Subreflector Beam Throw Calibration

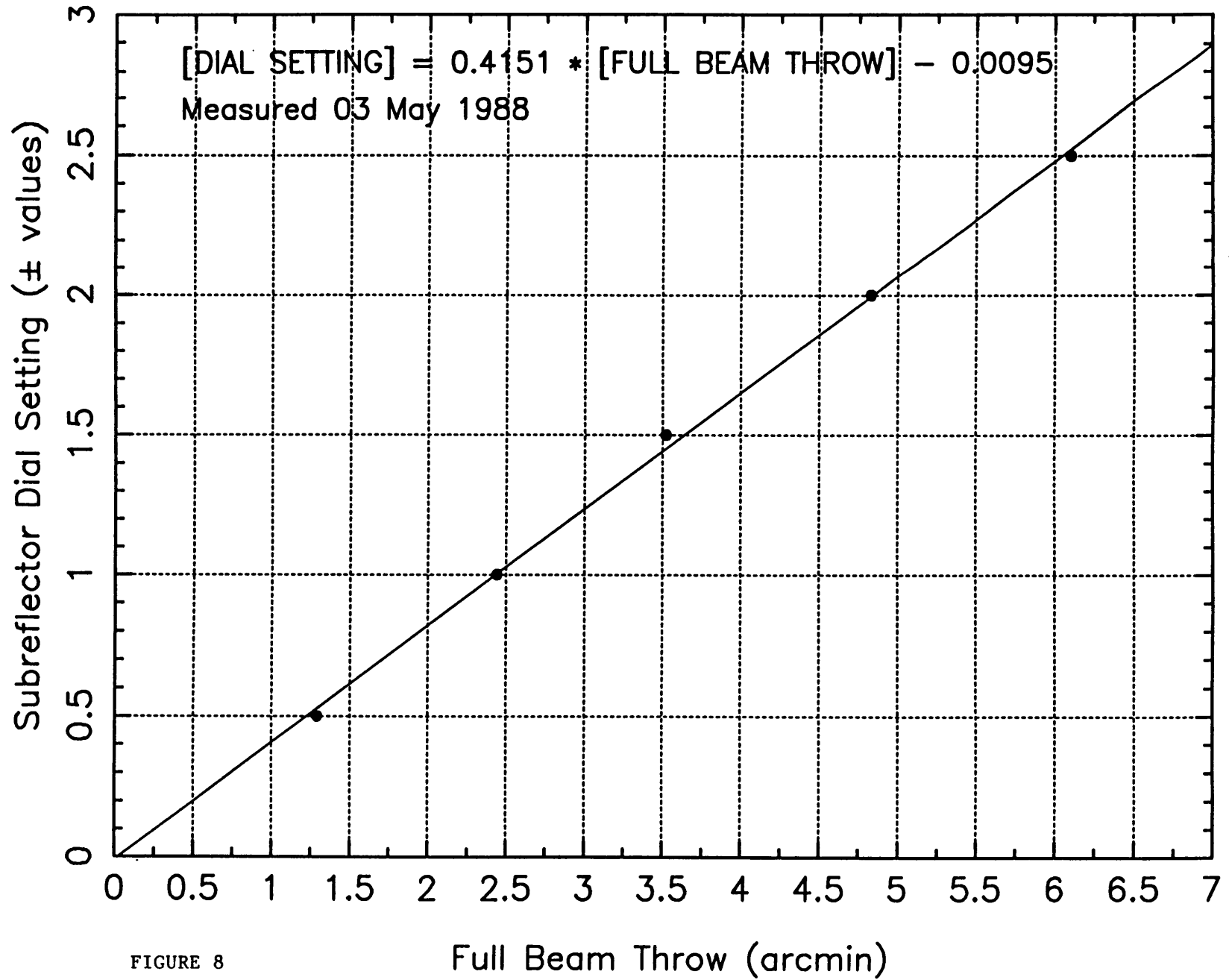


FIGURE 8

Aperture Efficiency

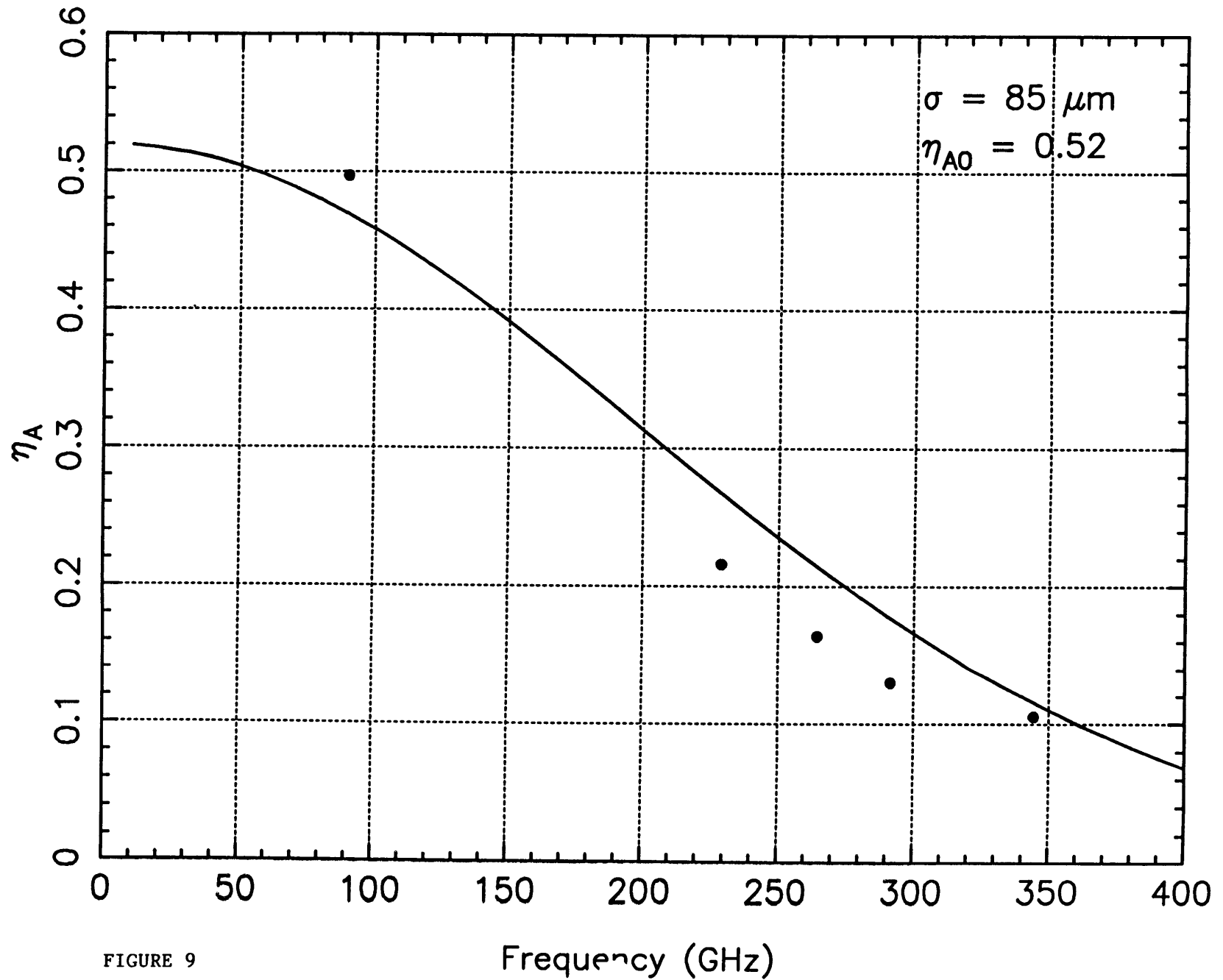


FIGURE 9

Standard Beam Efficiency

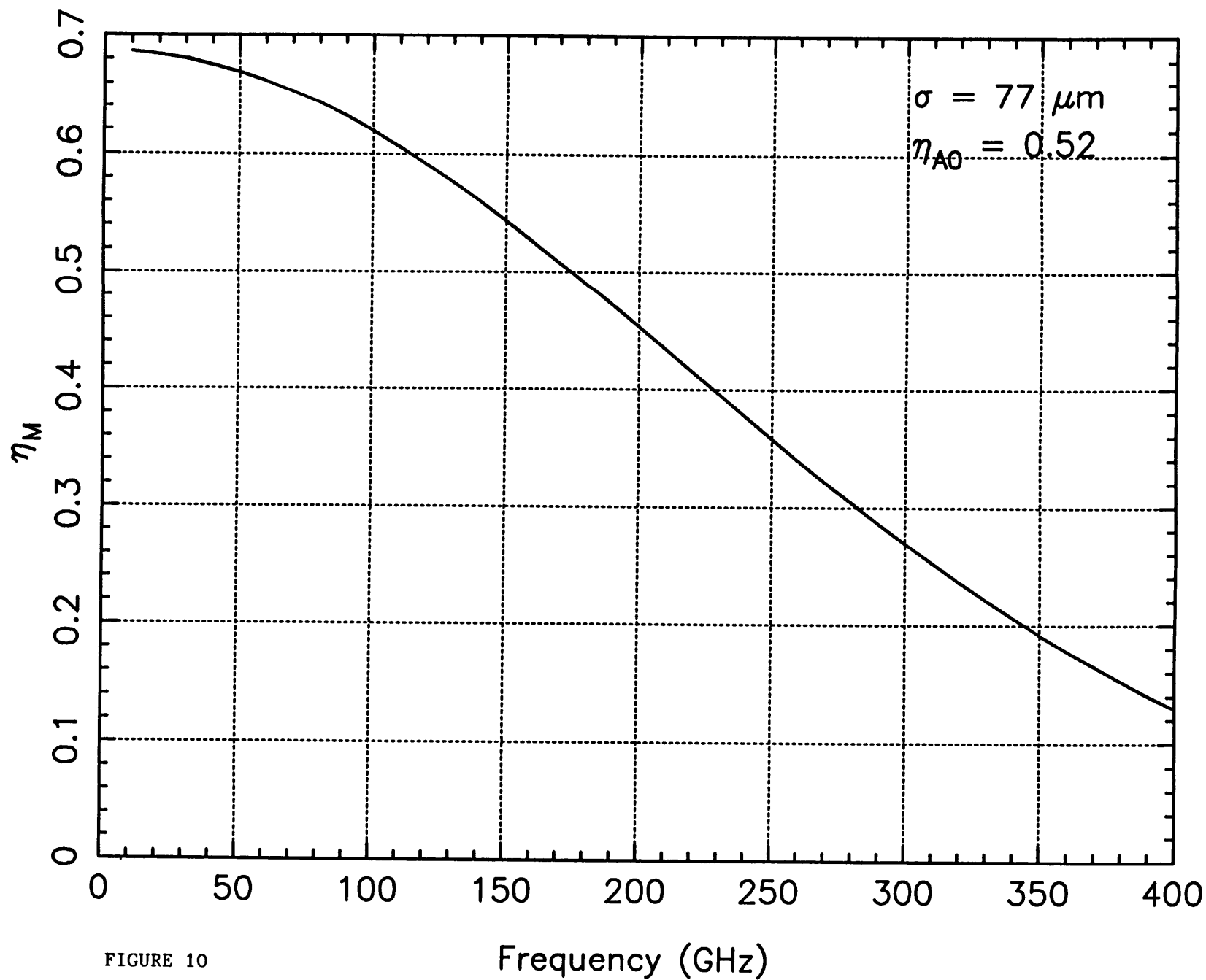


FIGURE 10

Main Diffraction Beamwidth (FWHM)

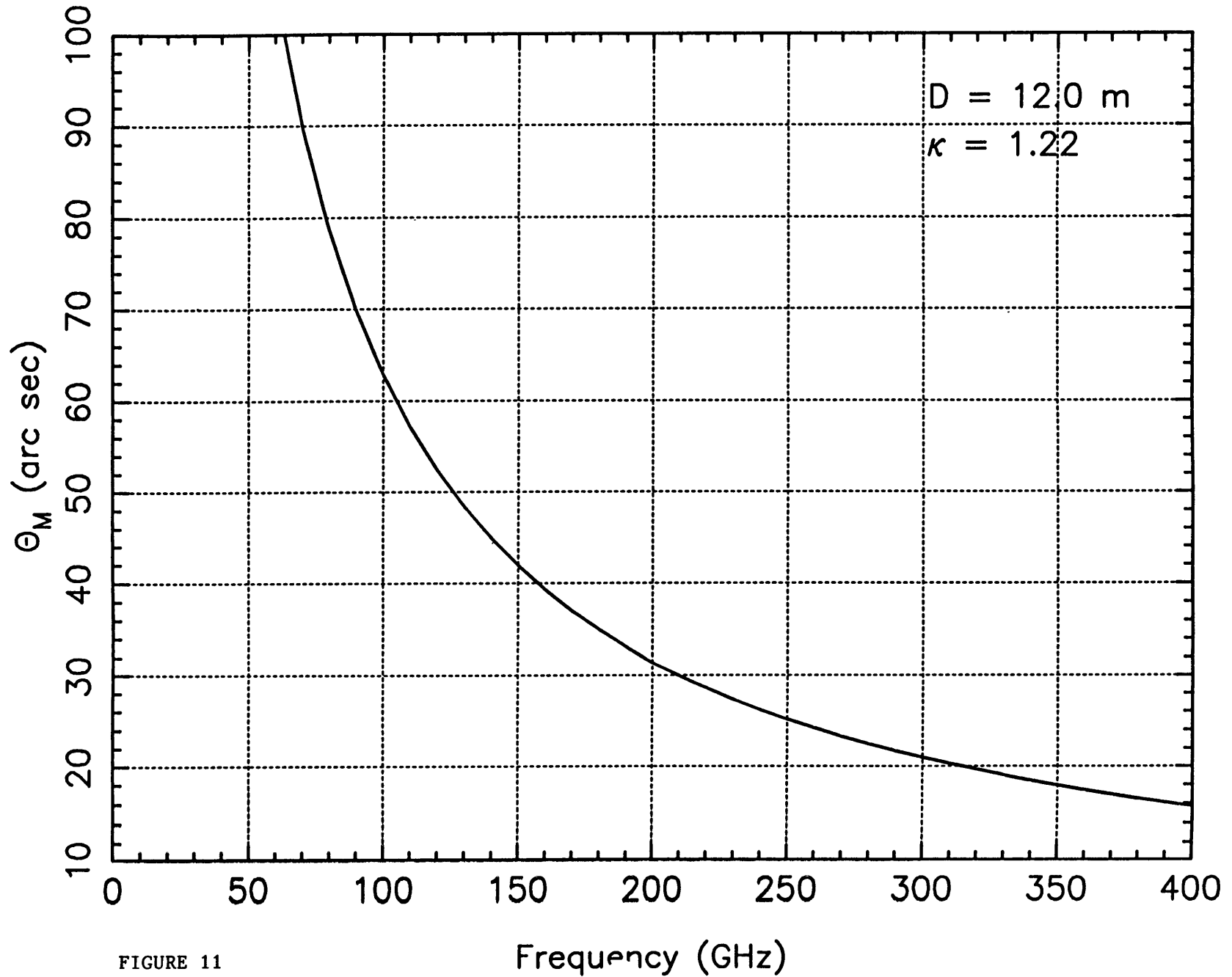


FIGURE 11

Janskys per Kelvin of T_A

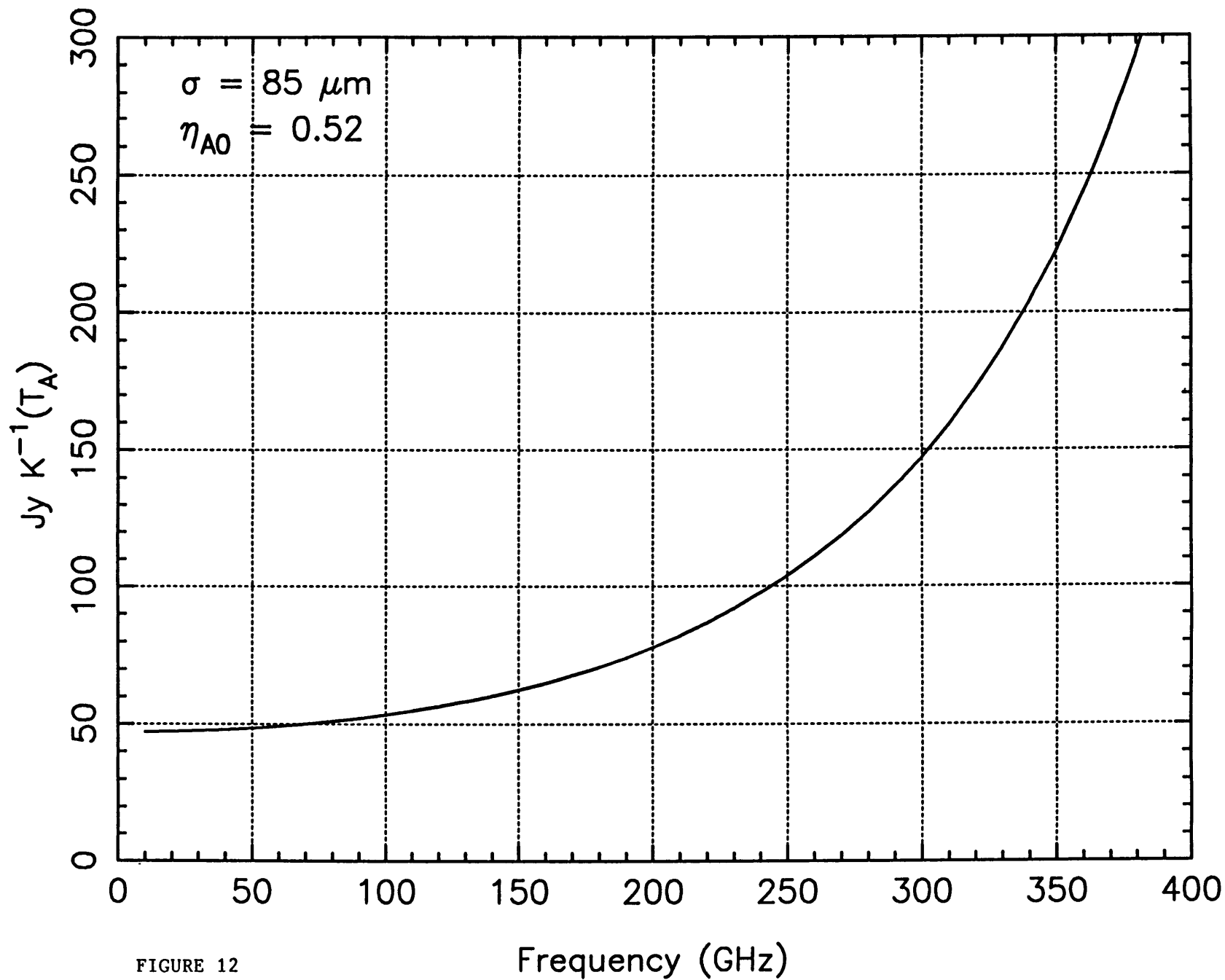


FIGURE 12

Janskys per Kelvin of T_R^* (For Vane Cal.)

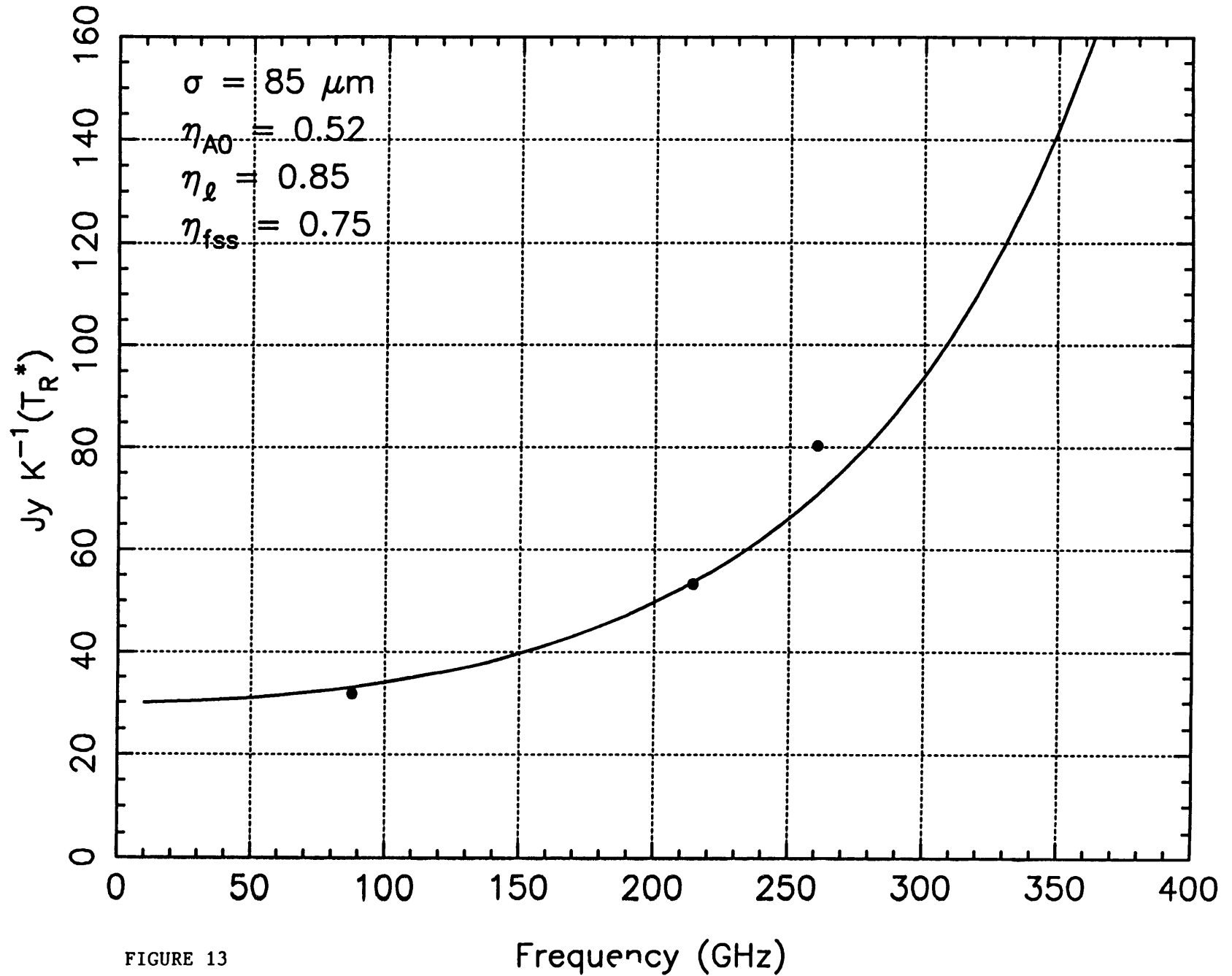


FIGURE 13

Corrected Beam Efficiency

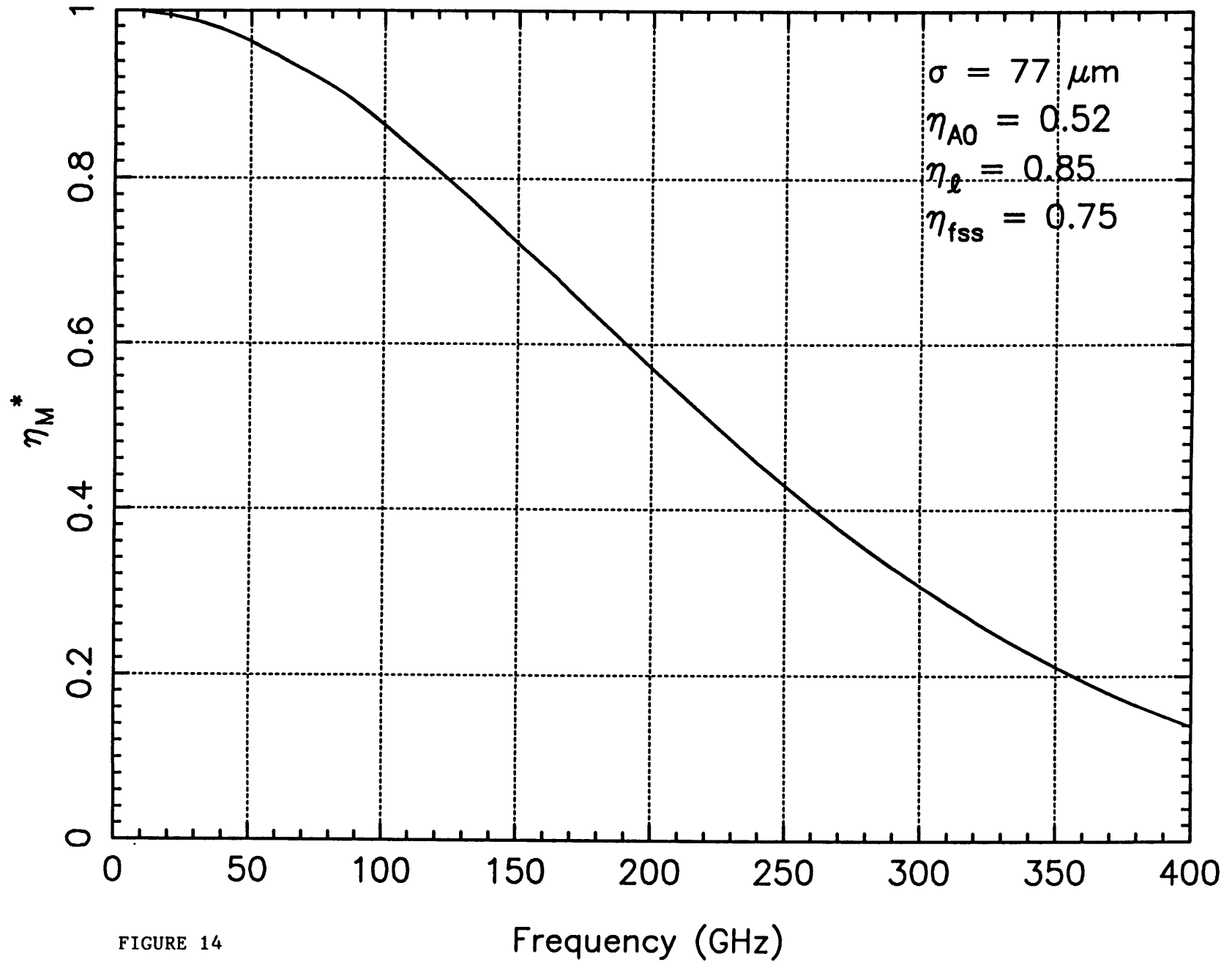


FIGURE 14

Error Beam FWHM

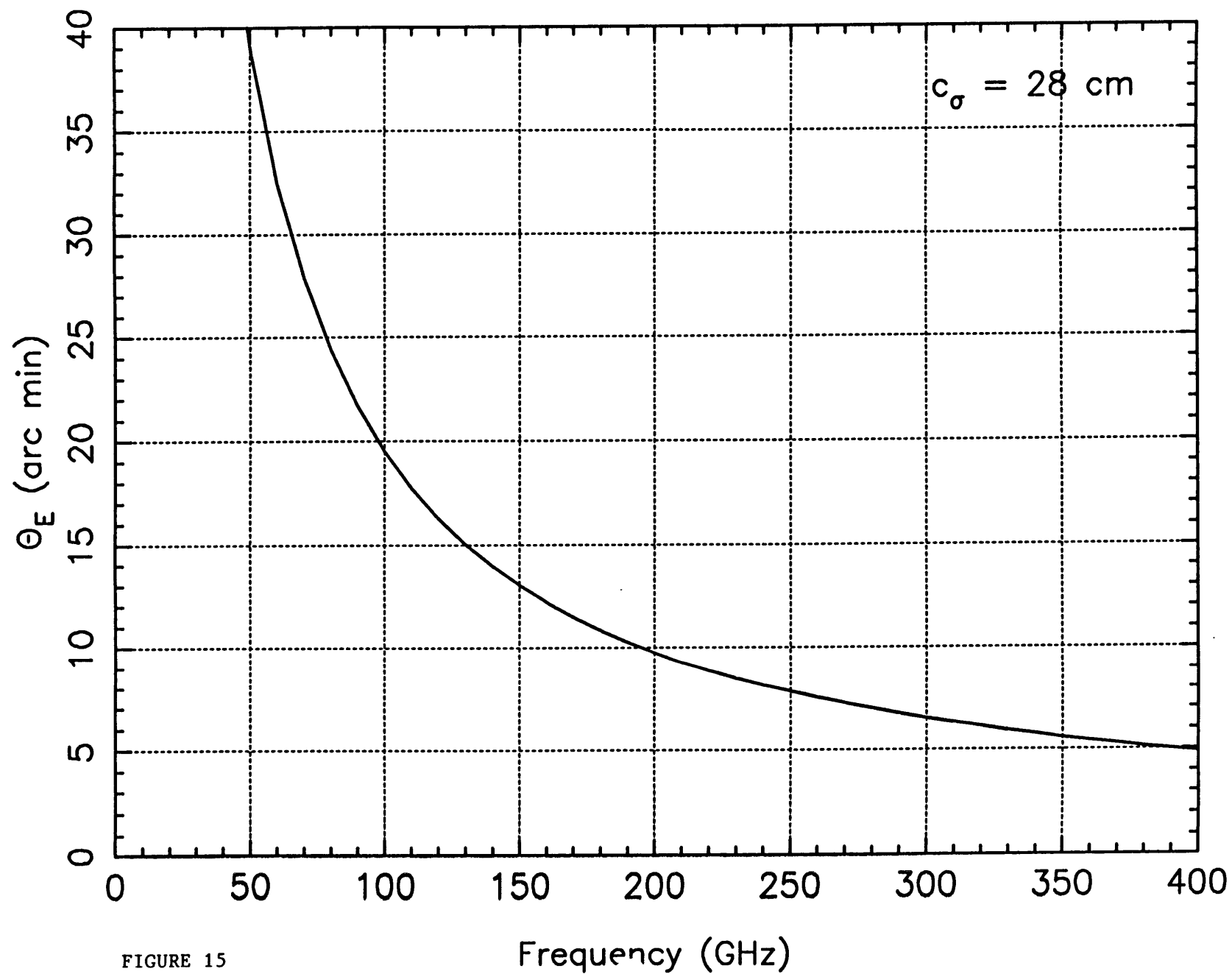


FIGURE 15

Ratio of Error Beam Amplitude to Main Beam Amplitude

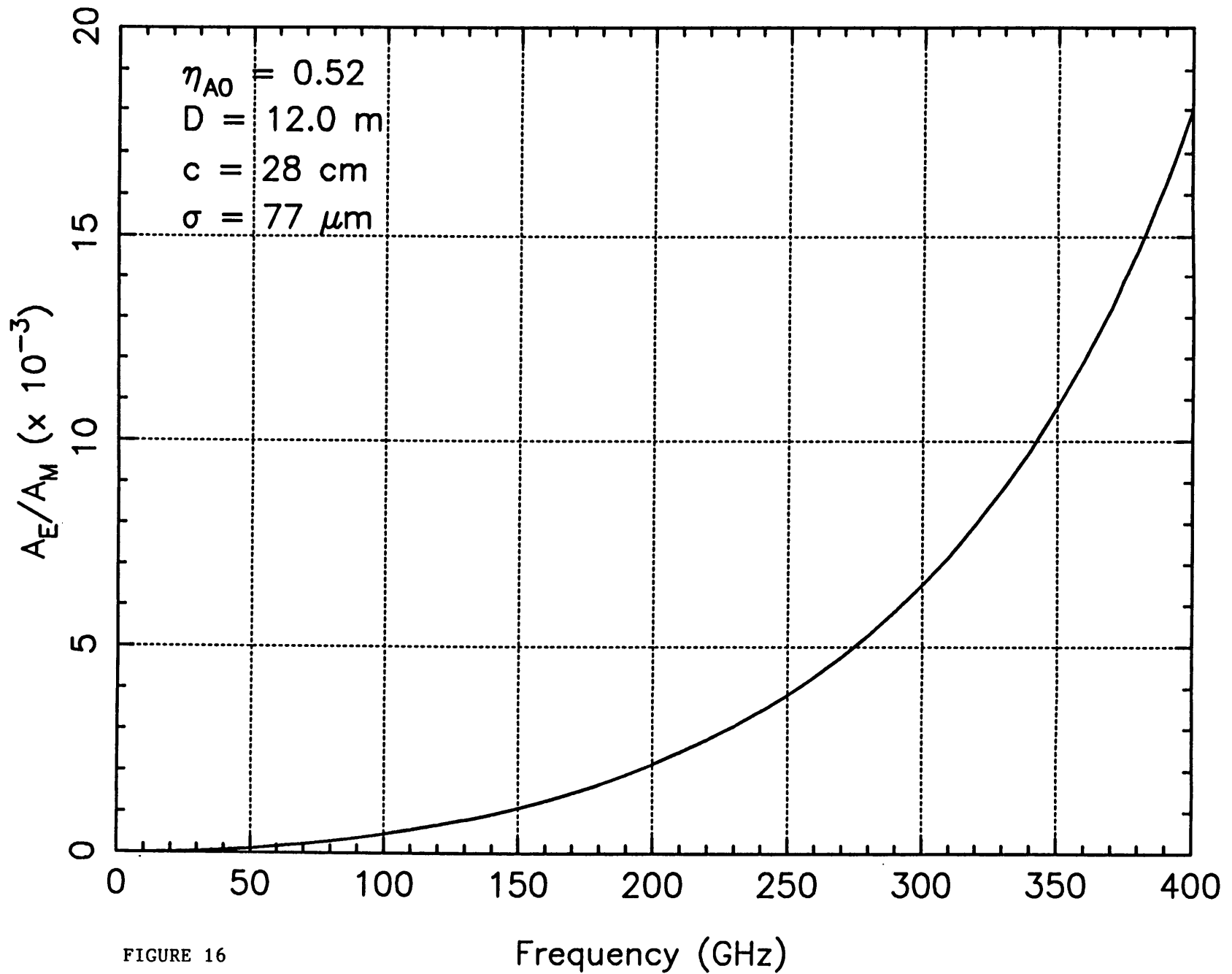


FIGURE 16

$\lambda 1.3$ mm Gain–Elevation Curve

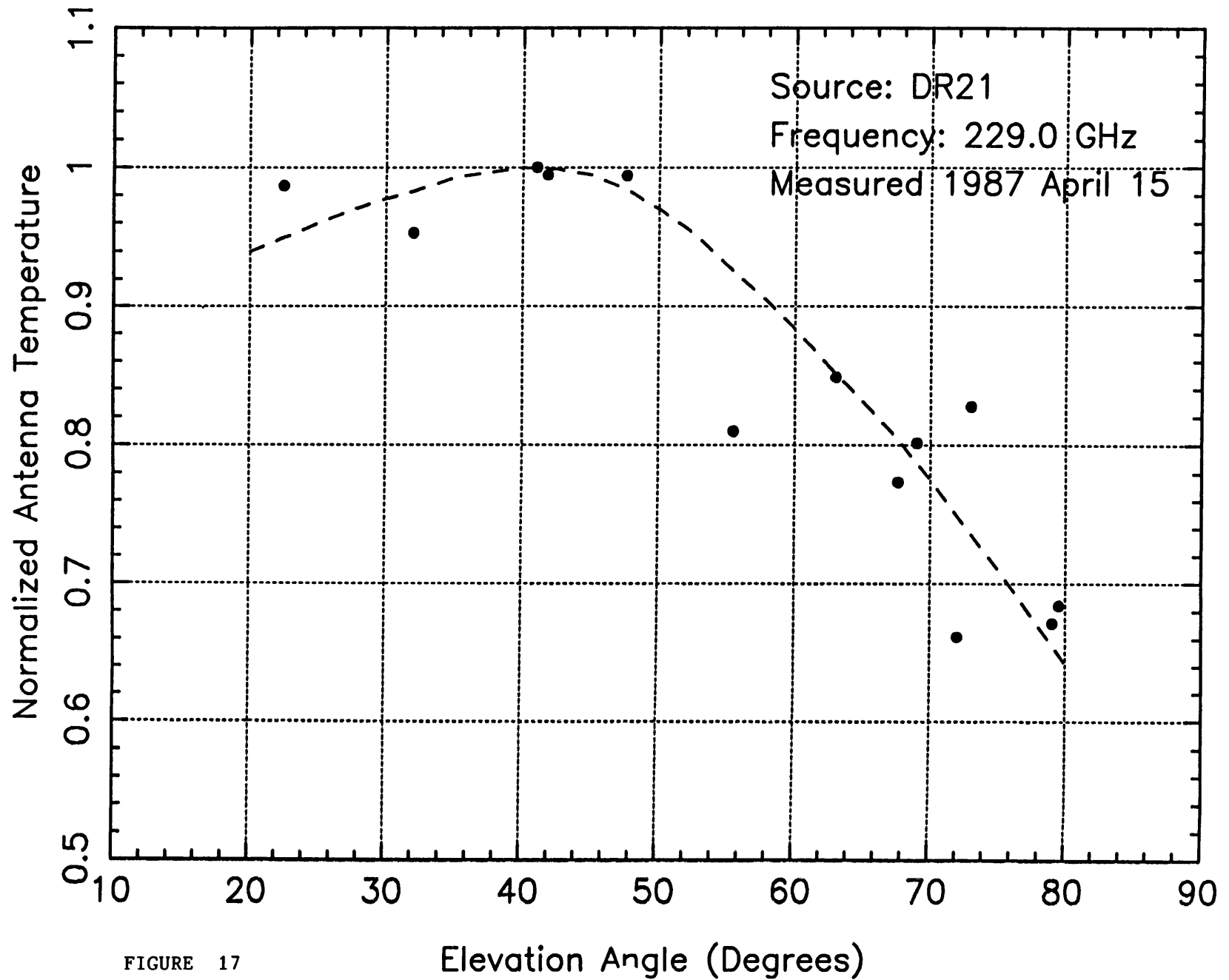


FIGURE 17